Near-tip stress rotation and the development of deformation band stepover geometries in mode II

Chris. H. Okubo[†]
Richard A. Schultz
Geomechanics–Rock Fracture Group, Department of Geological Sciences and Engineering/172, University of Nevada, Reno, Nevada 89557-0138, USA

ABSTRACT

The propagation of deformation bands into compressive and extensional stepover geometries is investigated by integrating field observations with numerical model simulations of the effective stress state due to shear along the bands. Deformation bands are tabular discontinuities, with mm- to cm-scale thicknesses, of localized volumetric strain and shear. Deformation bands are precursors to frictional slip (i.e., faulting) in porous granular rocks and soils. Systematic rotations in near-tip principal stress orientation due to shear along the overlapping deformation bands are shown to predict band propagation paths that are consistent with characteristic stepover geometries as viewed in the mode II direction, the orientation in which the observation plane is parallel with the displacement direction. Therefore, propagation paths for deformation bands can be predicted from knowledge of the effective near-tip stress state. These results establish a mechanics-based framework for investigations of fault growth and fault-controlled fluid flow in porous granular rocks and soils.

Keywords: deformation band, damage zone, plastic deformation, faulting, sandstone, stress rotation.

INTRODUCTION

In porous granular rocks and soils such as sandstone, limestone, or tuff, fault growth is preceded and accompanied by the development of damage zones of deformation bands (Jamison and Stearns, 1982; Shipton and Cowie, 2003). This process is analogous to the development of secondary fault-related fractures in crystalline rock. Deformation bands are tabular discontinuities that nucleate and propagate through localized shear (Aydin, 1978; Aydin and Johnson, 1978; Fig. 1). Deformation bands are a subset of a systematic range of structures that form at the onset of plastic yield in porous granular materials. Related plastic yield structures include dilation bands and compaction bands (localized volumetric strain with zero shear) and cataclastic flow (distributed volumetric and shear strain; Wong et al., 1997; Borja and Aydin, 2004; Schultz and Siddharthan, 2005).

The yield strength of a deformation band is smaller in magnitude than the peak strength of its host rock (Wong et al., 1997; Borja and Aydin, 2004; Schultz and Siddharthan, 2005). Therefore, deformation bands initially lack the discontinuous displacement fracture surfaces typical of joints and faults in crystalline rock. Deformation bands accumulate shear displacements independent of frictional (Coulomb) sliding. Typical shear strains measured across deformation bands in the field can be as much as 0.005 (maximum displacement to length ratio), and lengths of individual deformation bands may approach 100 m (Fossen and Hesthammer, 1997).

Deformation bands are precursors to the formation of through-going faults in porous granular rocks and soils. These bands accumulate shear strain independent of frictional sliding (i.e., faulting). Coulomb frictional slip can and does occur as a *secondary* process within the tabular thickness of the bands after sufficient (shear) strain-induced changes in the strength of the band material have occurred (Schultz and Siddharthan, 2005). Through-going faulting is accomplished by the linkage of these discontinuous patches of fault slip (Johnson, 1995; Shipton and Cowie, 2001).

Thus, deformation bands can evolve into faults, and the geometries of these faults are inherited from the geometries of the preexisting deformation bands (Aydin and Johnson, 1978; Antonellini and Aydin, 1994; Shipton and Cowie, 2001; Schultz and Balasko, 2003; Schultz and Siddharthan, 2005). Therefore, a mechanical understanding of deformation band stepover geometries is a key to investigating the growth and interaction of faults in porous granular rocks and soils. Faults and their surrounding damage zones also act as either barriers or

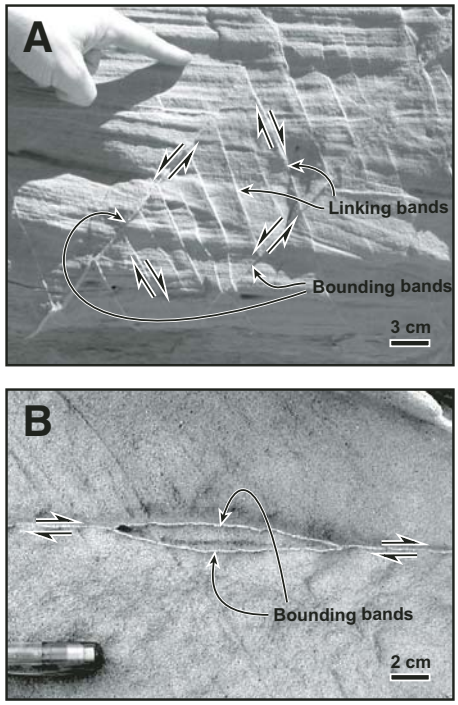

Figure 1. (A) Compressive and (B) extensional deformation band stepover geometries as viewed in the mode II direction. Deformation bands are the light-toned positive relief structures. The sense of offset is determined from displaced cross-bedding. Photographs taken in the Goblin Valley region of southern Utah. Host rock in both photos is Entrada Sandstone.

[†]Present address: Lunar and Planetary Laboratory, The University of Arizona, Tucson, Arizona 85721, USA; e-mail: chriso@pirl.lpl.arizona.edu.

GSA Bulletin; March/April 2006; v. 118; no. 3/4; p. 343–348; doi: 10.1130/B25820.1; 7 figures; 2 tables.

conduits to fluid flow (Antonellini and Aydin, 1994; Sigda and Wilson, 2003; Campbell et al., 2003). Accordingly, understanding the growth of deformation band stepover geometries also provides insight into the development of fluid flow patterns within structurally controlled reservoirs. The purpose of this paper is to show that the distinct geometries of deformation band stepovers are predictable from systematic variations in the local principal stress orientation ahead of propagating band tips.

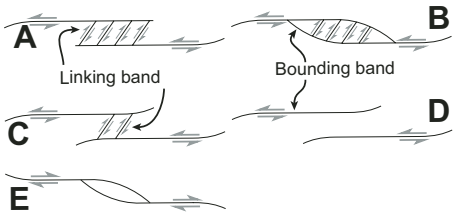

Figure 2. Commonly observed mode II deformation band stepover geometries showing the positions of the outer bounding bands and inner linking bands. Shown are compressive stepovers containing antithetic linking bands between (A) linear bounding bands (see also Fig. 1A) and (B) converging bounding bands, as well as diverging bounding bands with (C) and without (D) linking bands. Also shown is the geometry (E) of an extensional stepover (see also Fig. 1B).

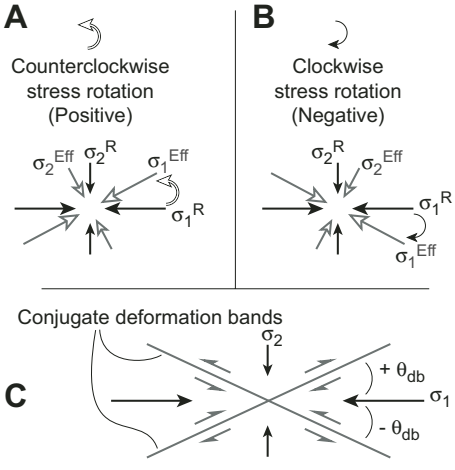

Figure 3. Sign conventions and angular metrics used in this paper. (A–B) Angle of stress rotation is measured from the prescribed remote principal stress orientation (e.g., σ_1^R) to the corresponding effective principal stress (e.g., σ_1^{Eff}), which is calculated as the sum of the remote principal stress plus the band-shear–induced local principal stress. The angle of stress rotation is thus the difference in orientation between σ_1^R and σ_1^{Eff}. (C) Geometric relationship of θ_{db} between σ_1 (either remote or effective) and both conjugate deformation band (db) orientations.

Field Observations

The scope of this paper is limited to the discussion of deformation band stepover structures as observed in the mode II direction (where the shearing vector is parallel with the observation plane; Fig. 1). Characteristic stepover geometries of deformation bands are observed at cm to 100 m scales and are seemingly invariant with scale; stepover geometries seen at the cm scale are also observed at the 100 m scale. The most distinct geometry of a mode II *compressive* stepover is characterized by a pair of "bounding" deformation bands that are connected by one or more antithetic "linking" deformation bands (Figs. 1A and 2A). Early work by Jamison and Stearns (1982) and by Davis et al. (2000) and coworkers interpret these antithetic linking bands as R′ Riedel shears along the two bounding bands. Schultz and Balasko (2003; see also Balasko, 2003) utilized field observations and numerical models to demonstrate that the antithetic linking bands are conjugate to the bounding bands and systematically grow within the stepover due to local stress concentrations between the actively propagating bounding bands.

Geometries that lack antithetic linking bands have been also observed in compressive (Fig. 2D) and extensional (Figs. 1B and 2E) deformation band stepovers. Du and Aydin (1993) used a criterion based on distortional strain energy density to predict the growth of these "simple" stepover geometries for both compressive and extensional deformation band stepovers. This criterion has also been used to reproduce particular stepover geometries for faults observed by Du and Aydin (1995).

Recently, Okubo and Schultz (2005) used yield criteria based on strain energy density to reproduce characteristic mode II geometries and intensities of 10-m-scale damage zones of deformation bands surrounding thrust faults within Wingate Sandstone. In that work, *volumetric* strain energy density is developed and verified as a criterion for quantifying the tendency for deformation band *nucleation* within these fault-related damage zones. Further, *distortional* strain energy density is shown to be an indicator of the tendency for deformation band *propagation* within these damage zones.

The contributions of Du and Aydin (1993) and Schultz and Balasko (2003) interpret deformation band propagation *tendency and direction* from numerical model calculations of distortional strain energy density. In these works, the tip of an individual deformation band is assumed to propagate toward the area of the maximum distortional strain energy density. Therefore, the resulting deformation bands would assume the overall geometries of the zones of elevated distortional strain energy density within the surrounding rock. Accordingly, the propagation direction of the deformation band would be independent of the orientation of the near-tip, effective maximum principal stress, σ_1^{Eff} (where σ_{ij}^{Eff} is the sum of the remote principal stress, σ_{ij}^{R}, plus the corresponding and coincident band-shear–induced local principal stress). Recent field observations and theoretical considerations show, however, that deformation bands propagate along conjugate angles, θ_{db}, from the σ_1^{Eff} direction (Fig. 3; Johnson, 1995; Borja, 2004; Borja and Aydin, 2004). Therefore, the deformation band propagation angle (i.e., θ_{db}) is tied to the orientation of σ_1^{Eff}, and variations in the σ_1^{Eff} orientation near the band tip may lead to changes in deformation band propagation *direction*. In this paper, we incorporate these recent and important findings to show that determining propagation direction from the near-tip σ_1^{Eff} orientation allows for the systematic investigation of subtle but key deformation band stepover geometries.

We commonly observe mode II deformation band stepover structures with the basic geometries shown in Figure 2. These geometries are based on detailed field observations of deformation band damage zones in the Sheets Gulch, Cottonwood canyon, Hillsdale canyon, Iron Wash, Goblin Valley and Molly's Castle areas of Utah, as well as at the Uncompahgre fold in western Colorado and at the Valley of Fire in southern Nevada.

Compressive stepovers with antithetic linking bands in which the bounding bands are subparallel (Figs. 1A and 2A) and intersect the opposite bounding band (Fig. 2B) are commonly observed. Also, compressive stepovers where the overlapping tips of the bounding bands diverge from the overlap (e.g., Du and Aydin, 1993) are also observed either with (Fig. 2C) or without (Fig. 2D) antithetic linking bands within the stepover. Isolated distal ends of the bounding bands (tip opposite from the stepover; tips A and D in Fig. 4) are observed to tend to curve toward the extensional quadrant as shown. Distal tips, however, commonly show stepover interactions with other adjacent bands, and examples of isolated distal tips are rare. These mode II geometries are typical of deformation band stepovers regardless of the global sense of shear across the bounding bands (normal, thrust, or strike-slip).

METHODOLOGY

In order to evaluate the effect of local stress rotations on the resulting stepover geometry, a series of numerical models using the 2-D boundary element code FAULT (Schultz, 1992) for elastic displacements in a full space are developed. FAULT has been used to calculate the results presented by Du and Aydin (1993, 1995), Schultz and Balasko (2003), and Okubo and Schultz (2005). Results of this study are based on the model setup of Schultz and Balasko (2003) with the geometry of Figure 4.

Deformation bands are modeled as seam elements (Crouch and Starfield, 1983, p. 208–210) that support continuous shear (nonfrictional) displacements across their ~1 mm thickness. The host rock is prescribed to have a Young's modulus of 18.2 GPa, shear modulus of 7.9 GPa, and Poisson's ratio of 0.15, consistent with porous sandstones (Lama and Vutukuri, 1978). The deformation bands have an equivalent (large-strain) shear modulus of 0.31 GPa, which is obtained from the magnitude of shear strain across the bands (Schultz and Balasko, 2003). Remote driving stress magnitudes are prescribed as $\sigma_1^R = 50$ MPa and $\sigma_2^R = 37.5$ MPa. This σ_1^R to σ_2^R ratio of 1.33 is less than the peak frictional strength of the host rock (~3, assuming typical friction coefficients of 0.6 or greater) and is sufficient to result in a shear displacement to band length ratio of 0.005 that is typical of natural bands (Fossen and Hesthammer, 1997). The results presented here use the counterclockwise positive (Fig. 3) and compression-positive sign conventions.

Conjugate deformation band orientations in Entrada Sandstone at the Goblin Valley and Molly's Castle areas in Utah suggest θ_{db} angles of 20°–30° (Johnson, 1995). Thus, deformation bands here would tend to propagate at conjugate orientations of ± ~25° from the σ_1^{Eff} direction. Based on these observations, we model a representative θ_{db} angle of 25°, recognizing that specific θ_{db} angles are dependent on the stress history of the host rock (e.g., Borja, 2004; Borja and Aydin, 2004). Compressive and extensional stepover geometries are simulated by varying the direction that σ_1^R acts in relative to the x-axis while keeping the band geometry the same: +25° for compressive stepovers, –25° for extensional stopovers (counterclockwise positive).

Stepover geometries with band separations of 0.45 cm and 1.8 cm are modeled, using overlap (*o*/*k*) and separation (*s*/*k*) ratios ranging from –6.7 to 26.7. These ratios are achieved by varying the position of band tip B (Fig. 4) while keeping all other tip positions constant. The results for models with overlap and separation ratios of 2.2 and 0.56 (Table 1) are representative of the entire parameter range and are discussed in detail here.

RESULTS AND DISCUSSION

In order to interpret our model results in terms of the resulting geometry of the deformation band stepover, we postulate (1) that deformation band propagation will occur in areas where the magnitude of distortional strain energy density is greater than the critical value necessary to induce plastic yielding (after Du and Aydin, 1993, 1995; Schultz and Balasko, 2003; and Okubo and Schultz, 2005), and (2) that the deformation band will propagate at the angle θ_{db} from the local σ_1^{Eff} direction. The latter premise is a key distinction from previous work (e.g., Du and Aydin, 1993, 1995; Schultz and Balasko, 2003) in which deformation bands are assumed to propagate toward regions of highest distortional strain energy density regardless of the orientation of the near-tip principal stresses.

Typical distributions of distortional strain energy density that are calculated by our numerical models are shown in Figure 5. These distributions are consistent with the results of Du and Aydin (1993, 1995) and Schultz and Balasko (2003). Concentrations of distortional strain energy density occur ahead of each band tip and along the plane of the band. Within the near-tip concentrations, magnitudes of distortional strain energy density approach 2.5 mega-Joules per cubic meter (MJ/m^3). Experimental testing of eolian Wingate Sandstone (similar in porosity and grain size/sorting to the Entrada Sandstone) suggests that a critical distortional strain energy density of ~1.27 MJ/m^3 is required to propagate deformation bands in this sandstone (Okubo and Schultz, 2005). Our numerical models produce values of distortional strain energy density that are larger than this critical value within the modeled space. Therefore, the magnitudes of distortional strain energy density within our models are assumed to be sufficient to promote propagation of the deformation bands.

Next, in order to evaluate the corresponding direction of propagation for these modeled deformation bands, we sample the σ_1^{Eff} orientations at 0.4 cm ahead of each band tip (Table 2). The sense of σ_1^{Eff} rotation at this distance is consistent with the orientations calculated at distances up to 0.6 cm ahead of the band tips. Results of this analysis are discussed separately for compressive and extensional stepover geometries.

Compressive Stepovers

In the modeled compressive stepover geometry, the calculated σ_1^{Eff} orientation ahead of each deformation band tip is rotated counterclockwise (Fig. 6A). This indicates that for the modeled geometry the deformation bands would tend to propagate away from the stepover (Fig. 6D). Growth of these bounding bands

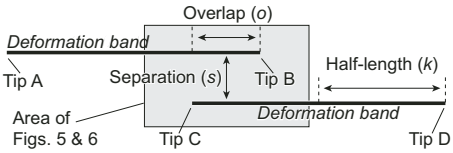

Figure 4. General geometry of the modeled deformation band stepovers. Specific model geometries are defined in Table 1 in terms of overlap, separation, and half-length for each segment defined by the shown tip labels.

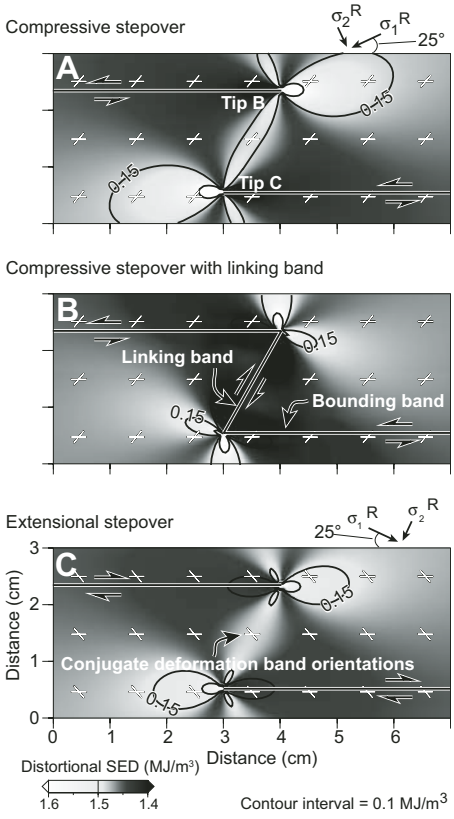

Figure 5. (A–C) Model-predicted conjugate deformation band orientations (inclined x marks) and distortional strain energy density (background). The tendency for deformation band propagation increases toward white. Predicted values of distortional strain energy density are everywhere greater than the minimum critical value typical for sandstone. Thus, these deformation bands are predicted to have sufficient energy to propagate in any direction within the modeled area.

TABLE 1. OVERLAP AND SEPARATION DATA FOR MODELED BAND GEOMETRIES DISCUSSED IN DETAIL IN THE TEXT

Segment	0.45 cm separation		1.8 cm separation	
	o/k	s/k	o/k	s/k
AB	0.20	0.09	0.20	0.36
CD	0.22	0.10	0.22	0.40

Note: Band CD has a constant length of 9 cm. o/k is the ratio of the band overlap distance (o) to the half-length of that band (k). s/k is the ratio of the band separation distance (s) to the half-length of that band (k). See Figure 4.

TABLE 2. PREDICTED ROTATION ANGLES OF σ_1^{EFF} ORIENTATIONS AHEAD OF THE MODELED DEFORMATION BAND TIPS (COUNTERCLOCKWISE POSITIVE)

Tip	0.45 cm separation	1.8 cm separation
	Angle of stress rotation (°)	
Extensional no linking band		
A	–0.58	–0.58
B	–0.51	–0.61
C	–0.51	–0.61
D	–0.58	–0.58
Compressive no linking band		
A	0.57	0.56
B	0.27	0.49
C	0.27	0.48
D	0.57	0.56
Compressive with linking band		
A	0.57	0.59
B	0.45	0.07
C	0.43	–0.58
D	0.57	0.59

Note: Tip labels refer to the geometry of Figure 5.

would result in the nonintersecting stepover geometry of Figure 2D.

Figure 5A shows the predicted conjugate orientations for deformation band propagation within the stepover. These conjugate orientations are rotated with the sense and magnitude that corresponds to the slight rotations in the principal stress orientation shown in Figure 6. The conjugate orientation that is subparallel with the orientation of the modeled bounding bands is the direction that these bounding bands would tend to propagate in. An antithetic linking band would propagate in the conjugate orientation to the bounding band (Schultz and Balasko, 2003). Therefore, although the bounding bands here do not show a tendency to converge, the calculated σ_1^{Eff} orientation does allow for the growth of antithetic linking bands within the stepover (e.g., Fig. 2C).

In order to test the effect of an antithetically oriented linking band on the propagation direction of the surrounding bounding bands in a compressive stepover, the model geometry of Figure 4 is modified to include an antithetic linking band between tips B and C (Fig. 5B). The model is calculated using the same parameters as defined in the Methods section, above. Results for the 1.8 cm separation model (Table 2) show that growth of an antithetic linking band has an important influence on the predicted propagation directions of the corresponding bounding bands.

With an antithetic linking band in place, tip B now shows negligible rotation of σ_1^{Eff} in the presence of the linking band. This means that tip B would tend to propagate in-plane, without converging or diverging from the stepover. This change in the propagation direction is due to the presence of the antithetic linking band within the stepover. A pair of bounding bands with similar in-plane propagation tendencies would produce the compressive stepover geometry shown in Figure 2A, which is consistent with the "backward-breaking" stepover geometry of Schultz and Balasko (2003).

Further investigation of the antithetic linking band model also shows that the propagation direction for tip C is predicted to have a clockwise rotation (Fig. 6B). This predicts that an antithetic linking band within the stepover would induce tip C to converge toward and intersect with the opposite bounding band (Fig. 6E). Mutually converging propagation directions for both bounding bands within a compressive stepover (necessarily with antithetic linking bands) would result in the geometry shown in Figure 2B. Therefore, our results suggest that in the 1.8 cm separation geometry, the presence of antithetic linking bands cause the overlapping bounding bands to tend to propagate in-plane (Figs. 1A and 2A) or to converge (Fig. 2B). In the absence of these antithetic linking bands, the overlapping bounding bands would tend to diverge (Fig. 6D).

We also test the effects of an antithetic linking band on the modeled stepover with smaller (0.45 cm) separation. Here, an antithetic linking band within the stepover is found to have a negligible effect on the propagation path of either overlapping tip. Unlike the larger 1.8 cm separation stepover, the bounding band tips in this less-separated stepover still have clockwise-rotated (diverging) propagation paths after addition of the antithetic linking band (Table 2). This result suggests that the amount of near-tip "counterrotation" of the bounding band propagation direction due to shear along an antithetic linking band is proportional to the length of that linking band, as modulated by the relative overlap and separation of the stepover.

Results of the larger 1.8 cm separation stepover model more specifically show that the *relative* bounding band length, as compared to the linking band length, controls the magnitude of the near-tip "counterrotation" of the bounding band propagation direction. Within this stepover, bounding band AB has a relative separation of 0.36, whereas bounding band CD has a slightly larger relative separation of 0.4. Thus band AB is longer than band CD, and band CD is longer than the antithetic linking band. This means that the difference in length between the antithetic linking band and band AB is greater than the difference in length between the antithetic linking band and band CD.

In the stepover with 1.8 cm separation, we clearly see that the σ_1^{Eff} orientations ahead of tip B are less counterrotated than the σ_1^{Eff} orientations ahead of tip C in the presence of the antithetic linking band (Table 2). These stress orientations are the sum of the remote stress plus the local stresses due to slip along the bounding and linking bands. This means that a longer linking band will have a greater effect on the effective stress orientation ahead of a bounding band, and a shorter linking band will have less of an effect. Thus, the length of the bounding band relative to the length of the linking band is a significant constraint on the magnitude of the "counterrotation" that the linking band will impart to propagation direction of the bounding band. Since the linking band is relatively much shorter to band AB than it is to band CD, the presence of the linking band has the least amount of influence on the effective stress orientation ahead of band AB.

Extensional Stepover

In extensional stepovers, the near-tip orientation of σ_1^{Eff} is rotated clockwise (Fig. 6C), leading to converging bounding band propagation directions (Fig. 6F). Between the overlapping bounding band tips, these propagation directions result in the "simple" extensional stepover geometry (Figs. 1B and 2E), in agreement with the model predictions of Du and Aydin (1993). Predicted σ_1^{Eff} orientations within the extensional stepover orient the plane conjugate to the bounding bands (i.e., the plane of the linking band) in a synthetic direction (Fig. 5C). Accordingly, and in line with field observations, antithetic linking bands are not predicted within extensional stepovers.

IMPLICATIONS

Results shown here demonstrate how the mode II geometry of through-going faults develops in porous granular rocks and soils. Detailed field observations consistently reveal that fault surfaces in porous granular rocks follow preexisting deformation band geometries (Aydin and

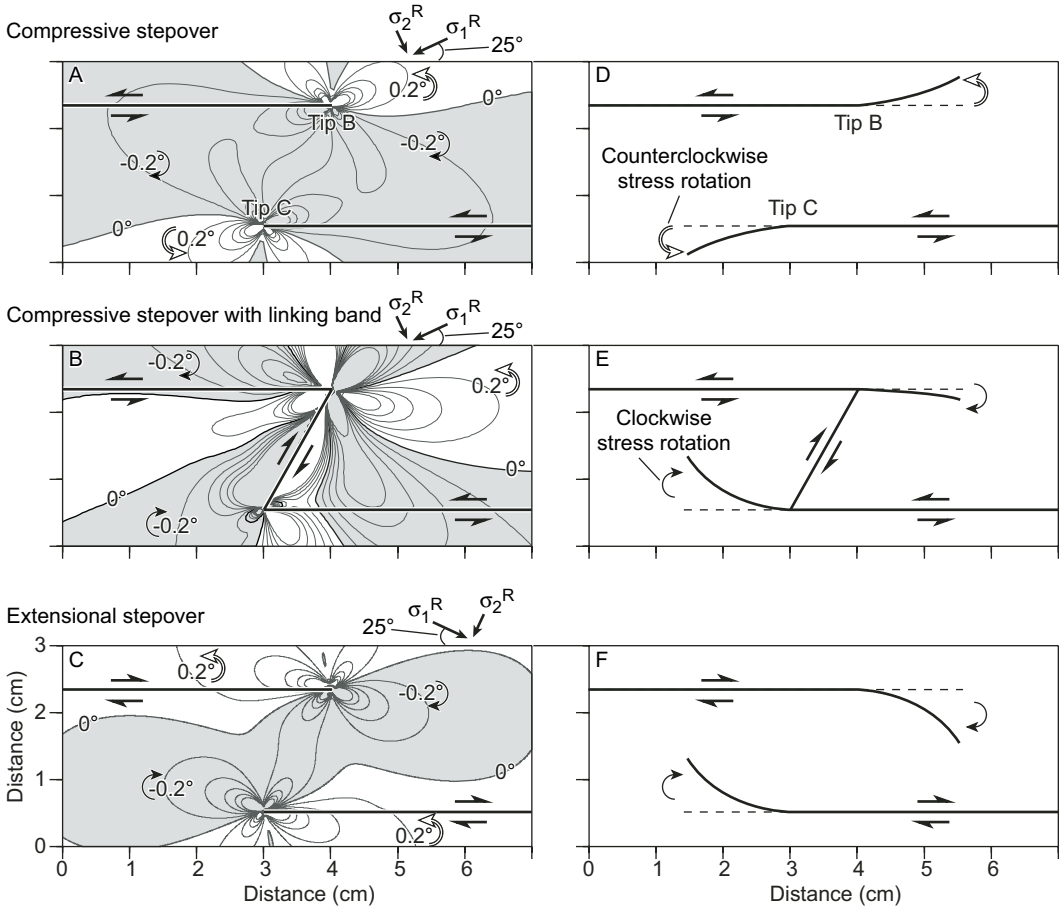

Figure 6. (A–C) Model-predicted effective principal stress rotation (contours). Shaded areas have clockwise stress rotations, and white areas have counterclockwise stress rotations. See Figure 2 for sign convention definition. (D–F) Representative bounding band geometries resulting from propagation under the corresponding effective principal stress orientations in views A–C.

Johnson, 1978; Antonellini and Aydin, 1994; Shipton and Cowie, 2001; Schultz and Balasko, 2003; Schultz and Siddharthan, 2005). Figure 7 shows the surface of a normal fault following along the bounding bands of multiple, meter-scale compressive stepovers with perquisite antithetic linking bands (i.e., geometry of Fig. 2B). The preexisting geometries of these compressive stepovers have imparted 10-cm-scale mode II corrugations to this section of the fault plane. This observation clearly illustrates how mode II fault geometry in granular rocks is a consequence of changes in σ_1^{Eff} orientations due to antecedent (or precursory) deformation band strain. Accordingly, this paper provides a framework for systematically investigating the development of mode II fault geometries in porous granular rocks. A detailed understanding of the mechanics that drive the geometry of faults in these rocks also provides insight into the distribution of fault-related damage zones of deformation bands (Jamison and Stearns, 1982; Okubo and Schultz, 2005), which are important controls on reservoir-scale fluid flow (Antonellini and Aydin, 1994; Sigda and Wilson, 2003).

CONCLUSIONS

Results presented here demonstrate that the near-tip principal stress orientation can be used to systematically reproduce characteristic bounding band propagation directions within compressive and extensional geometries of deformation band stepovers in mode II. Further, we show that the orientation of the principal stresses within these stepovers restricts the growth of antithetic linking bands to compressive stepovers. We show that the growth of antithetic linking bands within compressive stepovers leads to *subparallel* (Figs. 1A and 2A) or *converging* (Fig. 2B) bounding band tendencies. These bounding bands would tend to *diverge* (Fig. 2D) in the absence of the antithetic linking bands. The magnitude of this "counterrotation" in the bounding band propagation direction due to the presence of the antithetic linking band is found to be proportional to the relative length of that linking band. Relatively shorter linking bands (as within stepovers with smaller overlap and separation) exhibit less influence on the inherent diverging

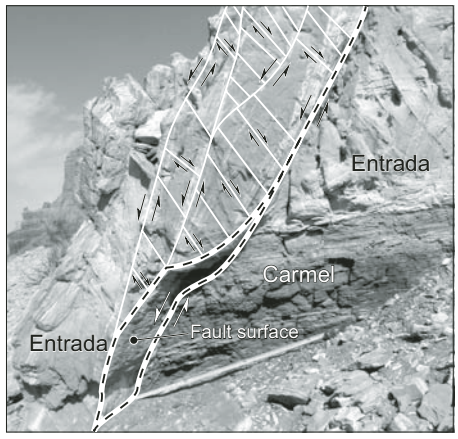

Figure 7. Frictionally slipping fault surface following the preestablished bounding band geometries of compressive stepovers (with antithetic linking bands). The normal sense of fault displacement juxtaposes Entrada Sandstone against siltstone of the Carmel Formation. Extended length of tape is 1 m. Photograph taken in the Molly's Castle region of southern Utah (UTM 0528200E, 4269585N, WGS84).

propagation directions of bounding bands in compressive stepovers.

ACKNOWLEDGMENTS

We thank Terry Engelder, Richard Schweickert, and two anonymous reviewers for constructive reviews of this manuscript. This work was supported by grants from the Planetary Geology and Geophysics Program of the National Aeronautics and Space Administration (NASA).

REFERENCES CITED

Antonellini, M., and Aydin, A., 1994, Effect of faulting on fluid flow in porous sandstones; petrophysical properties: American Association of Petroleum Geologists Bulletin, v. 78, p. 355–377.

Aydin, A., 1978, Small faults formed as deformation bands in sandstone: Pure and Applied Geophysics, v. 116, p. 913–930, doi: 10.1007/BF00876546.

Aydin, A., and Johnson, A., 1978, Development of faults as zones of deformation bands and as slip surfaces in sandstone: Pure and Applied Geophysics, v. 116, p. 931–942, doi: 10.1007/BF00876547.

Balasko, C.M., 2003, Mechanism and sequence of formation of deformation bands into spatially localized or distributed sets: Ladders, Riedels, and echelon arrays of Utah [M.S. thesis]: Reno, University of Nevada, 54 p.

Borja, R.I., 2004, Computational modeling of deformation bands in granular media. II. Numerical simulations: Computer Methods in Applied Mechanics and Engineering, v. 193, p. 2699–2718, doi: 10.1016/j.cma.2003.09.018.

Borja, R.I., and Aydin, A., 2004, Computational modeling of deformation bands in granular media. I. Geological and mathematical framework: Computer Methods in Applied Mechanics and Engineering, v. 193, p. 2667–2698, doi: 10.1016/j.cma.2003.09.019.

Campbell, K., Wolfsburg, A., Fabryka-Martin, J., and Sweetkind, D., 2003, Chlorine-36 data at Yucca Mountain: Statistical tests of conceptual models for unsaturated-zone flow: Journal of Contaminant Geology, v. 62–63, p. 143–161.

Crouch, S.L., and Starfield, A.M., 1983, Boundary Element Methods in Solid Mechanics: London, George Allen and Unwin, 322 p.

Davis, G.H., Bump, A.P., García, P.E., and Ahlgren, S.G., 2000, Conjugate Riedel deformation band shear zones: Journal of Structural Geology, v. 22, p. 169–190, doi: 10.1016/S0191-8141(99)00140-6.

Du, Y., and Aydin, A., 1993, The maximum distortional strain energy density criterion for shear fracture propagation with applications to the growth paths of en echelon faults: Geophysical Research Letters, v. 20, p. 1091–1094.

Du, Y., and Aydin, A., 1995, Shear fracture patterns and connectivity at geometric complexities along strike-slip faults: Journal of Geophysical Research, v. 100, p. 18,093–18,102, doi: 10.1029/95JB01574.

Fossen, H., and Hesthammer, J., 1997, Geometric analysis and scaling relations of deformation bands in porous sandstone: Journal of Structural Geology, v. 19, p. 1479–1493, doi: 10.1016/S0191-8141(97)00075-8.

Jamison, W.R., and Stearns, D.W., 1982, Tectonic deformation of Wingate Sandstone, Colorado National Monument: American Association of Petroleum Geologists Bulletin, v. 66, p. 2584–2608.

Johnson, A.M., 1995, Orientations of faults determined by premonitory shear zones: Tectonophysics, v. 247, p. 161–238, doi: 10.1016/0040-1951(95)00002-5.

Lama, R.D., and Vutukuri, V.S., 1978, Handbook on Mechanical Properties of Rocks, Vol. II: Testing Techniques and Results: Clausthal, Germany, Trans Tech Publications, 481 p.

Okubo, C.H., and Schultz, R.A., 2005, Evolution of damage zone geometry and intensity in porous sandstone: Insight gained from strain energy density: Journal of the Geological Society of London, v. 162, p. 939 950.

Schultz, R.A., 1992, Mechanics of curved slip surfaces in rock: Engineering Analysis with Boundary Elements, v. 10, p. 147–154, doi: 10.1016/0955-7997(92)90045-9.

Schultz, R.A., and Balasko, C.M., 2003, Growth of deformation bands into echelon and ladder geometries: Geophysical Research Letters, v. 30, doi: 10.1029/2002GL018449.

Schultz, R.A., and Siddharthan, R., 2005, A general framework for the occurrence and faulting of deformation bands in porous granular rocks: Tectonophysics (in press).

Shipton, Z.K., and Cowie, P.A., 2001, Damage zone and slip-surface evolution over μm to km scales in high-porosity Navajo sandstone, Utah: Journal of Structural Geology, v. 23, p. 1825–1844, doi: 10.1016/S0191-8141(01)00035-9.

Shipton, Z.K., and Cowie, P.A., 2003, A conceptual model for the origin of fault damage zone structures in high-porosity sandstone: Journal of Structural Geology, v. 25, p. 333–344, doi: 10.1016/S0191-8141(02)00037-8.

Sigda, J.M., and Wilson, J.L., 2003, Are faults preferential flow paths through semiarid and arid vadose zones?: Water Resources Research, v. 39, doi: 10.1029/2002WR001406.

Wong, T.-f., David, C., and Zhu, W., 1997, The transition from brittle faulting to cataclastic flow in porous sandstones: Mechanical deformation: Journal of Geophysical Research, v. 102, p. 3009–3025, doi: 10.1029/96JB03281.

Manuscript Received by the Society 12 March 2005
Revised Manuscript Received 4 August 2005
Manuscript Accepted 26 August 2005

Printed in the USA